Water Research 103 (2016) 74–82

Contents lists available at ScienceDirect

Water Research

journal homepage: www.elsevier.com/locate/watres

Bacteria attenuation by iron electrocoagulation governed by interactions between bacterial phosphate groups and Fe(III) precipitates

Caroline Delaire [a, *], Case M. van Genuchten [b], Susan E. Amrose [a], Ashok J. Gadgil [a, c]

[a] Department of Civil and Environmental Engineering, University of California, Berkeley, CA 94720-1710, United States
[b] Department of Earth Sciences – Geochemistry, Faculty of Geosciences, Utrecht University, Utrecht 3508TA, The Netherlands
[c] Energy Technologies Area, Lawrence Berkeley National Laboratory, Berkeley, CA 94720, United States

ARTICLE INFO

Article history:
Received 22 April 2016
Received in revised form
4 July 2016
Accepted 10 July 2016
Available online 11 July 2016

Keywords:
Iron electrocoagulation
Bacteria attenuation
Bacterial surface functional groups
Specific interactions
Bivalent cations
Oxyanions

ABSTRACT

Iron electrocoagulation (Fe-EC) is a low-cost process in which Fe(II) generated from an Fe(0) anode reacts with dissolved O_2 to form (1) Fe(III) precipitates with an affinity for bacterial cell walls and (2) bactericidal reactive oxidants. Previous work suggests that Fe-EC is a promising treatment option for groundwater containing arsenic and bacterial contamination. However, the mechanisms of bacteria attenuation and the impact of major groundwater ions are not well understood. In this work, using the model indicator *Escherichia coli* (*E. coli*), we show that physical removal via enmeshment in EC precipitate flocs is the primary process of bacteria attenuation in the presence of HCO_3^-, which significantly inhibits inactivation, possibly due to a reduction in the lifetime of reactive oxidants. We demonstrate that the adhesion of EC precipitates to cell walls, which results in bacteria encapsulation in flocs, is driven primarily by interactions between EC precipitates and phosphate functional groups on bacteria surfaces. In single solute electrolytes, both P (0.4 mM) and Ca/Mg (1–13 mM) inhibited the adhesion of EC precipitates to bacterial cell walls, whereas Si (0.4 mM) and ionic strength (2–200 mM) did not impact *E. coli* attenuation. Interestingly, P (0.4 mM) did not affect *E. coli* attenuation in electrolytes containing Ca/Mg, consistent with bivalent cation bridging between bacterial phosphate groups and inorganic P sorbed to EC precipitates. Finally, we found that EC precipitate adhesion is largely independent of cell wall composition, consistent with comparable densities of phosphate functional groups on Gram-positive and Gram-negative cells. Our results are critical to predict the performance of Fe-EC to eliminate bacterial contaminants from waters with diverse chemical compositions.

1. Introduction

Iron electrocoagulation (Fe-EC) is a process relying on the electrolytic dissolution of an Fe(0) anode to generate Fe(II), which is oxidized by dissolved O_2 to produce Fe(III) (oxyhydr)oxide precipitates with an affinity for microbial and chemical contaminants (Delaire et al., 2015; Tanneru and Chellam, 2012; van Genuchten et al., 2012). Fe-EC can efficiently remove arsenic from contaminated groundwater (Amrose et al., 2014; Li et al., 2012), and has also been shown to attenuate bacteria in a range of water matrices (Barrera-Díaz et al., 2003; Delaire et al., 2015; Ghernaout et al., 2008). In a recent study, we demonstrated that Fe-EC can attenuate *Escherichia coli* (*E. coli*) from synthetic Bengal groundwater (SBGW) without detriment to arsenic removal (Delaire et al., 2015), confirming that Fe-EC has promising applications for low-cost groundwater remediation (Amrose et al., 2014). Two processes contributed to bacteria attenuation in Fe-EC: (1) physical removal, caused by the adhesion of EC precipitates to cell walls, which results in bacteria enmeshment in Fe(III) flocs and subsequent settling, and (2) inactivation by reactive species produced upon Fe(II) oxidation by O_2. Fundamental aspects of the mechanisms underlying these two processes remain unknown. For example, the bacterial functional groups and the type of chemical interactions (electrostatic versus specific bonding) governing bacteria enmeshment in flocs are not well understood. In addition, the effect of major groundwater components, such as HCO_3^-, Ca, Mg, Si, and P, which can interfere with both inactivation and removal, has

* Corresponding author.
E-mail address: caroline.delaire@orange.fr (C. Delaire).

http://dx.doi.org/10.1016/j.watres.2016.07.020
0043-1354/

not been investigated. Finally, the impact of bacteria surface structure (Gram-positive versus Gram-negative, smooth versus rough Gram-negative) on attenuation has not been elucidated. By addressing these knowledge gaps, this study can improve considerably our predictions of Fe-EC performance in various water matrices containing different types of bacterial contamination.

Four types of surface functional groups are present on bacterial cell walls at comparable densities: hydroxyl (pK_a ~9.0), amine (pK_a ~9.0), carboxyl (pK_a ~4.7), and phosphate groups (pK_{a1} ~3.1, pK_{a2} ~6.6) (Borrok et al., 2005; Ngwenya et al., 2003). Hydroxyl and amine moieties do not have a strong affinity for Fe(III) oxides (McBride and Kung, 1991; Norén et al., 2008) and therefore they are not expected to strongly interact with EC precipitates. By contrast, carboxyl and phosphate moieties have strong affinities for Fe(III) oxides (Arai and Sparks, 2001; Chassé et al., 2015; Filius et al., 2000; van Genuchten et al., 2014a) and studies using Attenuated Total Reflectance Fourier-Transform Infrared spectroscopy (ATR-FTIR) have shown direct bonding of bacterial phosphate and carboxyl groups to hematite and goethite (Elzinga et al., 2012; Parikh and Chorover, 2006; Parikh et al., 2014). However, these studies were performed in controlled laboratory systems and simple water matrices, and they cannot be directly extrapolated to Fe-EC in groundwater, where precipitates and bacteria interact in an agitated suspension and in the presence of bivalent cations (Ca and Mg) and oxyanions (P and Si), which can sorb to bonding sites on bacteria (Beveridge and Koval, 1981; Johnson et al., 2007) and precipitates (van Genuchten et al., 2014b), respectively, and may therefore interfere with adhesion.

In addition to electrolyte composition, a number of studies have shown that the biomolecular structure of bacterial cell walls can affect their interactions with mineral surfaces through changes in surface charge, hydrophobicity, and steric hindrance (Chen and Walker, 2012; Jacobson et al., 2015; Walker et al., 2004). Because waterborne pathogenic bacteria and indicator organisms span the range of Gram-positive, smooth and rough (with and without O-antigen) Gram-negative strains (WHO, 2011), understanding the impact of cell wall structure on bacteria attenuation with Fe-EC is essential to generalize our findings to all bacterial species relevant to water quality.

Spectroscopic techniques such as ATR-FTIR, X-ray fluorescence (XRF) and X-ray absorption spectroscopy (XAS) have been used to study bacteria-Fe systems (Chan et al., 2009; Elzinga et al., 2012; Miot et al., 2009; Yan et al., 2016). However, these techniques cannot adequately determine bacteria-Fe(III) interactions in systems where Fe(III) is co-precipitated with bacteria in complex electrolytes similar to groundwater. For example, P–Fe bonds from bacteria-precipitate interactions and from aqueous P sorption to precipitates look very similar using ATR-FTIR (Elzinga et al., 2012) and would not be distinguishable with P K-edge XAS (Kelly et al., 2008). Additionally, ATR-FTIR is not suited to investigate interactions taking place inside large flocs due to the low penetration length of infrared beams in aqueous medium (~1 μm). To circumvent these limitations, the present study proposes an innovative approach, where macroscopic data of bacteria attenuation in systematically varied electrolytes are combined with ζ-potential measurements to elucidate the molecular interactions between bacteria and EC precipitates. Although this approach can only provide indirect evidence for specific interactions between bacteria and precipitates, it builds upon previous spectroscopic studies, which have identified bacteria-Fe oxide bonding processes in simple controlled systems (Elzinga et al., 2012; Parikh and Chorover, 2006; Parikh et al., 2014) and structures of Fe-EC precipitates in complex water matrices (van Genuchten et al., 2014a, 2014b), to gain information about bacteria removal mechanisms in groundwater-like electrolytes.

The goals of this study are to: (1) determine the impact of HCO_3^-, Ca, Mg, P, and Si on bacteria attenuation with Fe-EC, (2) identify the bacterial functional groups involved in the adhesion of EC precipitates to cell walls and investigate the type of interaction (electrostatic versus specific), and (3) test the generalizability of these conclusions to various bacteria types. To achieve these objectives, we first compared Fe-EC with $FeCl_3$ coagulation to distinguish the contributions of inactivation and removal via enmeshment in flocs to overall bacteria attenuation in Fe-EC as a function of the HCO_3^- concentration. Inactivation results were confirmed using live-dead staining. Second, we systematically investigated the effect of ionic strength, Ca/Mg, and P/Si on *E. coli* attenuation, both in single and in multiple solute electrolytes, to constrain the bacterial functional groups involved in precipitate adhesion to cell walls. ζ-potential, a proxy for surface charge, was used to assess the interaction of major groundwater ions with the surface of EC precipitates or *E. coli* cells. Third, we validated our proposed mechanism with 3 bacteria strains bearing different surface structures (smooth and rough Gram-negative, and Gram-positive). Our results strongly suggest that Fe-EC can be used to remove various types of bacteria from a wide range of water matrices representative of regions affected by arsenic and microbial contamination of groundwater. More generally, this study can help predict the performance of Fe-EC, and other Fe-based coagulation processes, to reduce bacterial contaminants from drinking water and wastewater.

2. Methods

2.1. Bacteria preparation and enumeration

One Gram-positive and two Gram-negative bacterial strains were used: *Enterococcus faecalis* (ATCC 19433, no antibiotic resistance), *Escherichia coli* K12 (NCM 4236, kanamycin-resistant), and *Escherichia coli* ECOR 10 (from STEC center, ampicillin-resistant (Mazel et al., 2000)). K12 is a rough strain (no O-antigen) (Stevenson et al., 1994) whereas ECOR 10 is a smooth strain (O-antigen present, serotype O6) (STEC center, 2016). After three propagations in growth media amended with appropriate antibiotics, stationary-phase bacteria were rinsed 3 times and resuspended in 100 mM NaCl as detailed in the Supporting Information. Bacteria were spiked in Fe-EC electrolytes to achieve initial concentrations of $10^{6.1-6.7}$ CFU/mL ($10^{5.0-5.8}$ CFU/mL for *E. faecalis*). Bacteria concentrations were enumerated in duplicate in 0.1 mL aliquots as colony forming units (CFU) using the spread plate technique on agar amended with appropriate antibiotics (detection limit of 10 CFU/mL), as described in the Supporting Information.

2.2. Electrolytes

The list of electrolytes used in bacteria attenuation experiments is specified in Table S1. In summary, we first varied the concentration of HCO_3^- (0.1–8.0 mM) to examine its impact on bacteria inactivation. Second, a range of ionic strengths was investigated by varying NaCl (in deionized water and in SBGW) or $NaClO_4$ (in 1 mM $CaCl_2$). Then, concentrations of bivalent cations (Ca: 0–13.5 mM and Mg: 0–10.6 mM) and oxyanions (P: 0–0.4 mM and Si: 0–0.4 mM) were systematically varied, in single and composite electrolytes, to elucidate their effect on bacteria removal. Finally, SBGW containing 8.2 mM HCO_3^-, 2.7 mM Ca, 2.0 mM Mg, 1.3 mM Si, 0.15 mM P, and 6.3 μM As(III), was prepared as described elsewhere (Delaire et al., 2015) and used as the electrolyte in some experiments. All experiments were conducted at pH 7.0 ± 0.3, except for the comparisons between the three bacterial strains, which were conducted at pH 7.5 ± 0.2. The pH was held constant throughout experiments by adding HCl, NaOH or $NaHCO_3$ as needed.

Electrolytes were selected in part to overlap with previous work on the structure of EC precipitates (van Genuchten et al., 2014a, 2014b, 2012), which we leverage in our interpretations of bacteria attenuation and ζ-potential measurements.

2.3. Fe-EC and $FeCl_3$ experiments

The procedure used for Fe-EC experiments has been described elsewhere (Delaire et al., 2015) and is detailed in the Supporting Information. Briefly, two 1 cm × 8 cm Fe(0) electrodes were submerged in 200 mL of electrolyte spiked with bacteria (anodic submerged area of 3 cm^2). In all experiments, a current density of 10 mA/cm^2 was applied for 11 min, resulting in a Faradaic Fe dosage of 0.5 mM, which was chosen to result in a range of detectable post-treatment *E. coli* concentrations. After the electrolysis stage, suspensions were stirred open to the atmosphere for 90–180 min to allow for complete Fe(II) oxidation and formation of Fe(III) precipitates. Suspensions were then left to settle overnight to separate individual cells from cells associated with EC precipitates. When required for floc formation and settling (Table S1), 5 mg/L-Al of $Al_2(SO_4)_3$ (alum) was added at the end of the mixing period, along with approximately 1.5 mM $NaHCO_3$ to avoid a pH drop. Preliminary tests confirmed that the addition of alum did not significantly modify bacteria attenuation (see Supporting Information). Solution pH was not controlled during the settling stage. In a subset of experiments, coagulation by $FeCl_3$ addition was used instead of Fe-EC to isolate the contribution of removal from that of inactivation. In these experiments, 1 mL of a 100 mM $FeCl_3$ solution was added to the electrolyte and the solution pH, which dropped to ~3 during $FeCl_3$ addition, was re-adjusted to 7.0 ± 0.1 in less than 5 min.

Unfiltered and filtered (0.45 μm nylon filters) samples were taken before Fe-EC, and before and after overnight settling, for measurements of Fe, As, Ca, Mg, P, and Si by inductively coupled plasma optical emission spectrometry (ICP–OES, PerkinElmer 5300 DV, measurement error typically < 5%). All samples for ICP-OES analysis were digested in 0.2 M HCl. Filtered and unfiltered samples were used to measure Fe(II) and total Fe (Fe(II) + Fe(III)), respectively (Delaire et al., 2015). Across the 113 bacteria attenuation experiments reported here, the total Fe concentration after Fe-EC (Fe dosage) was 96% ± 7% of the value predicted by Faraday's law (0.5 mM). Unoxidized Fe(II) (before settling) and unsettled Fe (after settling) were <1.2% and <4.7% of the total Fe dosed, respectively. Because the formation of calcite, magnesite, or hydroxyapatite in our experiments was limited if not negligible (see Supporting Information), Ca/Mg/P removal measured by ICP-OES was used as a proxy for Ca/Mg/P uptake by EC precipitates. Bacteria attenuation was calculated as the difference between log CFU concentrations before Fe-EC and after settling (samples taken from the supernatant, ~3 cm below the surface), and therefore accounts for both inactivation and removal via enmeshment in flocs. Bacteria attenuation experiments were generally replicated three or more times, except for 12 experiments conducted in duplicate or less (see Table S2). We report average bacteria attenuations ± one standard deviation across replicates.

Finally, to assess the effect of P/Si on the uptake of carboxyl moieties by EC precipitates, we performed citrate removal experiments using Fe-EC in the presence and absence of oxyanions under conditions identical to *E. coli* removal experiments, using 10 mg/L-Al of alum before settling (Table S1). Citrate concentrations were measured as total C with a TOC-V_{CSH} analyzer (Shimadzu).

2.4. ζ-potential measurements and bacterial viability tests

In this study, ζ-potential measurements, which are a proxy for surface charge, were used to track the impact of major groundwater ions on the surface of EC precipitates or *E. coli K12* cells. ζ-potential was measured by dynamic light scattering (Malvern Zetasizer Nano-ZS) at 633 nm. In addition, qualitative assessments of membrane permeabilization, which were used as a proxy for bacteria inactivation, were performed with the BacLight LIVE-DEAD kit (Invitrogen) used in conjunction with fluorescent microscopy (Zeiss AxioImager, 63× Plan-Apochromat objective, EndoGFP and mCherry filters, UC Berkeley CNR Biological Imaging Facility). Sample preparation and data collection procedures are described in the Supporting Information.

2.5. Model of Ca/Mg complexation by bacterial cell walls

Drawing on previous work (Johnson et al., 2007; Ngwenya et al., 2003), we derived a simple equilibrium surface complexation model, which included three bivalent cation adsorption sites on bacterial cell walls: carboxyl groups, protonated and deprotonated phosphate groups. The model predicts the percentage of bacterial phosphate and carboxyl groups complexed by Ca and Mg as:

$$\%_{P\ groups\ complexed} = \frac{K_{P1,Ca}[Ca^{2+}] + K_{P1,Mg}[Mg^{2+}] + \frac{K_{A2}}{[H^+]}\left(K_{P2,Ca}[Ca^{2+}] + K_{P2,Mg}[Mg^{2+}]\right)}{\frac{[H^+]}{K_{A1}} + 1 + \frac{K_{A2}}{[H^+]} + K_{P1,Ca}[Ca^{2+}] + K_{P1,Mg}[Mg^{2+}] + \frac{K_{A2}}{[H^+]}\left(K_{P2,Ca}[Ca^{2+}] + K_{P2,Mg}[Mg^{2+}]\right)} * 100 \quad (1)$$

$$\%_{C\ groups\ complexed} = \frac{K_{C,Ca}[Ca^{2+}] + K_{C,Mg}[Mg^{2+}]}{\frac{[H^+]}{K_A} + 1 + K_{C,Ca}[Ca^{2+}] + K_{C,Mg}[Mg^{2+}]} * 100 \quad (2)$$

Deprotonation constants of bacterial surface functional groups and Ca adsorption constants were obtained directly from the literature (Johnson et al., 2007). Mg adsorption constants were derived from a relationship between metal-acetate and metal-bacteria complexation constants proposed by Johnson et al. (Johnson et al., 2007). Additional details regarding the derivation of this model, including equilibrium constants, are given in the Supporting Information and Table S3.

3. Results and discussion

3.1. Effect of HCO_3^- on the contributions of removal and inactivation

The effect of 8 mM HCO_3^- on *E. coli* attenuation by Fe-EC and $FeCl_3$ coagulation is shown in Fig. 1a. Representative images of live-dead stained *E. coli* are presented in Fig. 1b–e. Whereas 8 mM HCO_3^- did not significantly affect *E. coli* attenuation by coagulation with $FeCl_3$, the presence of HCO_3^- decreased attenuation by Fe-EC by ~1.2

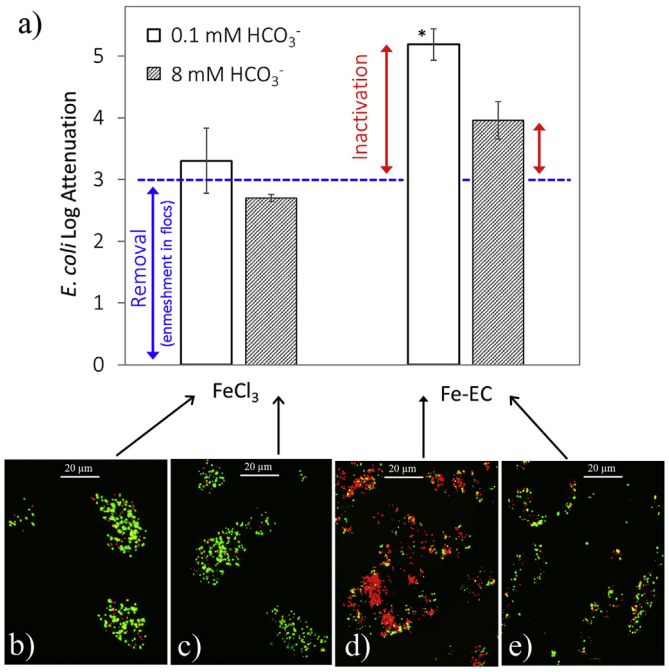

Fig. 1. *E. coli* attenuation with Fe-EC and $FeCl_3$, with and without 8 mM HCO_3^-. Fe dosage was 0.5 mM in all experiments. Panel a shows *E. coli* log attenuations. The asterisk indicates that the detection limit for bacteria attenuation was reached for some of the replicate experiments. Panels b–e show fluorescent microscopy images of live (green)-dead (red) stained *E. coli* cells. The blue dashed line is the average attenuation in all $FeCl_3$ experiments (with and without HCO_3^-) and represents removal (blue arrow). *E. coli* log attenuations are compared to this baseline to deduce approximate log inactivations (red arrows). All experiments were conducted at pH 7.0. In 0.1 mM HCO_3^- experiments, 2 mM NaCl were added for conductivity. (For interpretation of the references to colour in this figure legend, the reader is referred to the web version of this article.)

log. Because no Fenton-type reactive oxidants are produced from an Fe(III) salt – due to the absence of Fe(II) – (Hug and Leupin, 2003), minimal inactivation occurs during $FeCl_3$ coagulation (consistent with live-dead staining, Fig. 1b and c), which implies that attenuation via $FeCl_3$ addition is exclusively due to physical removal (enmeshment in flocs). In addition, Fe-EC and $FeCl_3$ coagulation generate precipitates with virtually identical structures and surface properties (Li et al., 2014; Roberts et al., 2004; van Genuchten et al., 2012). Therefore, $FeCl_3$ coagulation can be used as a proxy for bacteria removal in Fe-EC. Consequently, the difference in attenuations between Fe-EC and $FeCl_3$ coagulation can be attributed to inactivation.

As shown in Fig. 1a, HCO_3^- did not affect physical removal, which is consistent with ζ-potential measurements showing that HCO_3^- does not significantly interact with the surface of *E. coli* cells or Fe(III) precipitates (Fig. S1). By contrast, 8 mM HCO_3^- decreased inactivation substantially by ~1.2 log (Fig. 1a), consistent with significantly lower membrane permeabilization (Fig. 1d and e). Therefore, because inactivation is likely to be a marginal attenuation process in carbonated waters, we do not focus on a deep investigation of inactivation mechanisms in this work. However, we speculate that membrane damage may be caused by reactive intermediates such as $O_2^{\bullet-}$, H_2O_2, and Fe(IV), which are generated during Fenton-type reactions (Hug and Leupin, 2003; Keenan and Sedlak, 2008) and have been associated with bactericidal effects (Alt et al., 1999; Ikawa et al., 2010; Kim et al., 2010). The $CO_3^{\bullet-}$ radical, which is produced when HCO_3^- or Fe(II)-carbonate complexes react with H_2O_2 (Hug and Leupin, 2003; Medinas et al., 2007) is much more reactive and therefore shorter-lived than $O_2^{\bullet-}$, H_2O_2, and Fe(IV) (Augusto and Miyamoto, 2011; Jacobsen et al., 1998; Neta et al., 1988) (see Supporting Information). Thus, the inhibition of inactivation by HCO_3^- might be explained by a shift in the nature of reactive species produced during Fe-EC towards a shorter-lived oxidant ($CO_3^{\bullet-}$) that is more likely to die off in the bulk than to interact with cell membranes.

Overall, Fig. 1 shows that both inactivation and removal (via enmeshment in flocs) contribute to *E. coli* attenuation in Fe-EC, and that the concentration of HCO_3^- governs the amount of inactivation. In the remaining sections of our study, we will focus on removal. Interactions between EC precipitates and *E. coli* cells are investigated by varying levels of ionic strength, Ca, Mg, P, and Si. Because these ions are not expected to react with oxidants such as $O_2^{\bullet-}$, H_2O_2, or Fe(IV) (Hug and Leupin, 2003; Li et al., 2012; Roberts et al., 2004), nor to interact with lipid aliphatic chains, which are the target of oxidants on cell membranes (lipid peroxidation), they are assumed to have a negligible effect on inactivation. Therefore, their potential impact on *E. coli* attenuation will be solely attributed to changes in removal.

3.2. Effect of ionic strength

Increasing ionic strength over 2 orders of magnitude (2–200 mM), which results in increased charge screening (Debye length decreased tenfold), did not significantly affect *E. coli* attenuation by Fe-EC, regardless of the initial electrolyte composition (Fig. S2). The negligible effect of ionic strength suggests that electrostatic interactions play a secondary role compared to specific interactions in the adhesion of EC precipitates to *E. coli* cells. In the following two sections, we investigate the bacterial surface sites involved in these interactions by systematically varying the concentration of bivalent cations and oxyanions in order to selectively complex adsorption sites on the surface of *E. coli* cells and EC precipitates, respectively.

3.3. Effect of bivalent cations: Ca and Mg

3.3.1. Single solute electrolytes (no oxyanions, no HCO_3^-)

E. coli attenuation as a function of Ca and Mg concentrations is shown in Fig. 2a. Ca and Mg both decreased *E. coli* attenuation, with a larger inhibitory effect observed for Mg (2.1 log decrease in attenuation when Mg increased from 0 to 10.6 mM) than for Ca (1.3 log decrease in attenuation when Ca increased from 0 to 12.9 mM). Because bivalent cations should not affect inactivation (see Section 3.1.), these reductions in bacteria attenuation can be interpreted as reductions in *E. coli* removal.

Fig. 2b shows the ζ-potential of EC precipitates and *E. coli* cells as a function of Ca/Mg concentrations. In this single Ca/Mg solute electrolyte, EC precipitates were positively charged. Increasing concentrations of Ca/Mg had a limited effect on the ζ-potential of precipitates, suggesting that bivalent cations interacted minimally with their surface, consistent with unchanged settling velocity at higher Ca/Mg concentrations. This result was expected given the repulsive electrostatic forces between bivalent cations and positively-charged EC precipitates, and is consistent with previous work showing negligible uptake of Ca/Mg by Fe(III) (oxyhydr)oxides at circumneutral pH in the absence of oxyanions (Kanematsu et al., 2013; Stachowicz et al., 2008). By contrast, Ca and Mg caused a significant increase in the ζ-potential of *E. coli* cells, indicating a strong interaction between bivalent cations and bacteria surfaces. Fig. S3 shows the percentage of bacterial functional groups complexed by bivalent cations, as predicted by our equilibrium surface model. According to this model, raising Ca/Mg concentrations from 0 to 13 mM leads to a significant increase in the complexation of carboxyl (from 0 to 70–80%) and phosphate

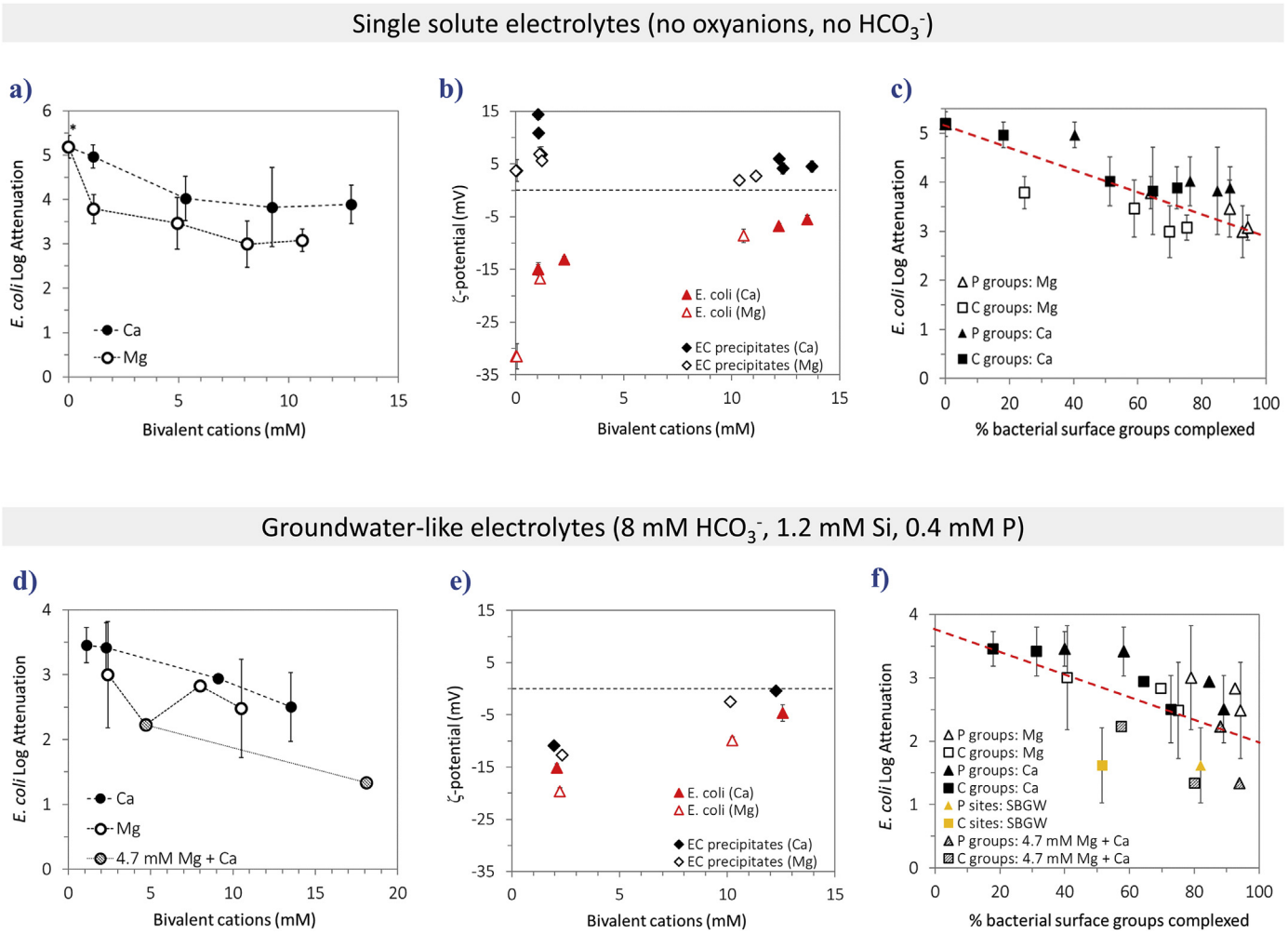

Fig. 2. Effect of Ca and Mg on *E. coli* attenuation in Fe-EC, in single solute electrolytes (panels a, b and c) and in groundwater-like electrolytes containing 8 mM HCO_3^-, 1.2 mM Si, and 0.4 mM P (panels d, e and f). Panels a and d: effect of increasing Ca/Mg concentrations on *E. coli* log attenuation with an Fe dosage of 0.5 mM. The asterisk indicates that the detection limit for bacteria attenuation was reached for some of the replicate experiments. Panels b and e: effect of increasing Ca/Mg concentrations on the ζ-potential of EC precipitates and *E. coli* cells (data points for 0 mM Ca and 0 mM Mg overlap on panel b). Panels c and f: *E. coli* attenuation as a function of complexed bacterial surface groups (combination of .panel a and S3, and panel d and S3, respectively). The dotted red lines highlight the inverse correlation between *E. coli* attenuation and the complexation of bacterial functional groups. All experiments were conducted at pH 7.0. Experiments with no Ca/Mg (panel a) were conducted in 2 mM NaCl for conductivity. (For interpretation of the references to colour in this figure legend, the reader is referred to the web version of this article.)

(from 0 to 90–95%) groups, which is consistent with the observed increase in *E. coli* ζ-potential (Fig. 2b).

Fig. 2c combines *E. coli* attenuation results (Fig. 2a) and model outputs (Fig. S3) to highlight that *E. coli* removal decreases as the percentage of complexed bacterial carboxyl and phosphate groups increases. Stronger inhibition of *E. coli* removal by Mg than by Ca (Fig. 2a) is consistent with this trend, because Mg has a higher affinity for bacterial surface functional groups (Beveridge and Koval, 1981) (Table S3 and Fig. S3).

3.3.2. *Groundwater-like electrolytes (with oxyanions and HCO_3^-)*

Fig. 2d shows the effect of Ca (0–13.5 mM) and Mg (2.4–10.5 mM) on *E. coli* attenuation in a groundwater-like electrolyte containing 8 mM HCO_3^-, 1.2 mM Si, and 0.4 mM P. Similar to the single Ca/Mg solute system, bivalent cations reduced *E. coli* attenuation, with Ca/Mg concentrations above 10 mM leading to a 1–2 log decrease in attenuation.

Fig. 2e shows ζ-potentials of EC precipitates and *E. coli* cells as a function of Ca/Mg concentrations in the groundwater-like electrolyte. Bivalent cations increased the ζ-potential of *E. coli* cells, consistent with the complexation of phosphate and carboxyl groups on cell walls, as explained in Section 3.3.1. In this electrolyte, EC precipitates were negatively-charged due to the sorption of P and, to a lesser extent, Si (P:Fe and Si:Fe molar solids ratios of 0.7 ± 0.1 and 0.06 ± 0.04, respectively) (Appenzeller et al., 2002; Hamid et al., 2011). In contrast to previous experiments in the absence of oxyanions, bivalent cations significantly interacted with the surface of EC precipitates in the groundwater-like electrolyte, as indicated by a substantially higher ζ-potential at larger Ca/Mg concentrations. This increase in precipitate surface charge coincided with increased Ca/Mg uptake, with solids ratios going from 0.5 ± 0.1 to 1.2 ± 0.7 mol Ca:mol Fe, and from 0.3 ± 0.1 to 0.5 ± 0.4 mol Mg:mol Fe, respectively. EC precipitates with similar chemical compositions (i.e. Ca/Mg:P:Fe molar ratios) have been documented in previous studies performed in nearly identical electrolytes, but in the absence of bacteria (van Genuchten et al., 2014a, 2014b). In these studies, Ca was shown to interact with P sorbed to Fe(III) precipitates, via direct Ca–O–P bonds, and to a lesser extent, electrostatically. In the present study, the observed increase in precipitate ζ-potential with Ca/Mg in the groundwater-

like electrolyte is consistent with such interactions of Ca/Mg with P sorbed to EC precipitates.

Fig. 2f illustrates the inverse relationship between *E. coli* attenuation in the groundwater-like electrolyte and the percentage of bacterial functional groups complexed by Ca/Mg (derived from our model). Fig. 2f also includes data from our previous study of *E. coli* attenuation in SBGW containing 2.6 mM Ca and 1.9 mM Mg (Delaire et al., 2015), which are consistent with this trend. Finally, we note that *E. coli* attenuations in groundwater-like electrolytes (Fig. 2f) were overall ~1 log lower than in single solute systems (Fig. 2c), which is consistent with the inhibition of inactivation by 8 mM HCO_3^- shown in section 3.1.

Taken together, Fig. 2a–f show that Ca/Mg decreases *E. coli* removal independent of the electrolyte, and more specifically, independent of the surface charge of EC precipitates: whether Ca/Mg increase (Fig. 2b, no oxyanions) or decrease (Fig. 2e, oxyanions present) the electrostatic barrier to precipitate adhesion on cell walls, bivalent cations equally inhibit *E. coli* removal. Combined with the limited impact of ionic strength (Section 3.2 and Fig. S2), this result confirms the minimal role of electrostatic interactions on *E. coli* removal and instead points to the importance of specific interactions between EC precipitates and bacterial phosphate and/or carboxyl groups. These findings are in good agreement with previous ATR-FTIR studies that provided evidence for direct bonding between Fe oxides and bacterial phosphate/carboxyl groups in more simple and controlled systems (Elzinga et al., 2012; Parikh and Chorover, 2006; Parikh et al., 2014).

3.4. Effect of oxyanions: P and Si

3.4.1. Single solute electrolytes (no bivalent cations, no HCO_3^-)

Fig. 3a shows the effect of 0.4 mM Si/P on *E. coli* attenuation in electrolytes containing no Ca/Mg. Whereas Si had no detectable effect, P reduced *E. coli* attenuation by 1.6 log. Because Si and P should not affect inactivation, as explained in Section 3.1, these effects correspond to changes in removal via enmeshment in flocs. ζ-potential measurements of EC precipitates and *E. coli* cells as a function of P/Si concentrations are presented in Fig. 3b. Si and P had no detectable effect on the ζ-potential of *E. coli* cells, reflecting the absence of interaction between these oxyanions and bacterial cell walls. By contrast, Si and P significantly decreased the ζ-potential of EC precipitates, indicating oxyanion sorption (Appenzeller et al., 2002; Hamid et al., 2011), which is supported by the uptake of Si and P measured by ICP-OES (Si:Fe and P:Fe molar solids ratios of 0.3 and 0.6, respectively). Because electrostatic interactions do not play a major role in *E. coli* removal, as demonstrated above, lower

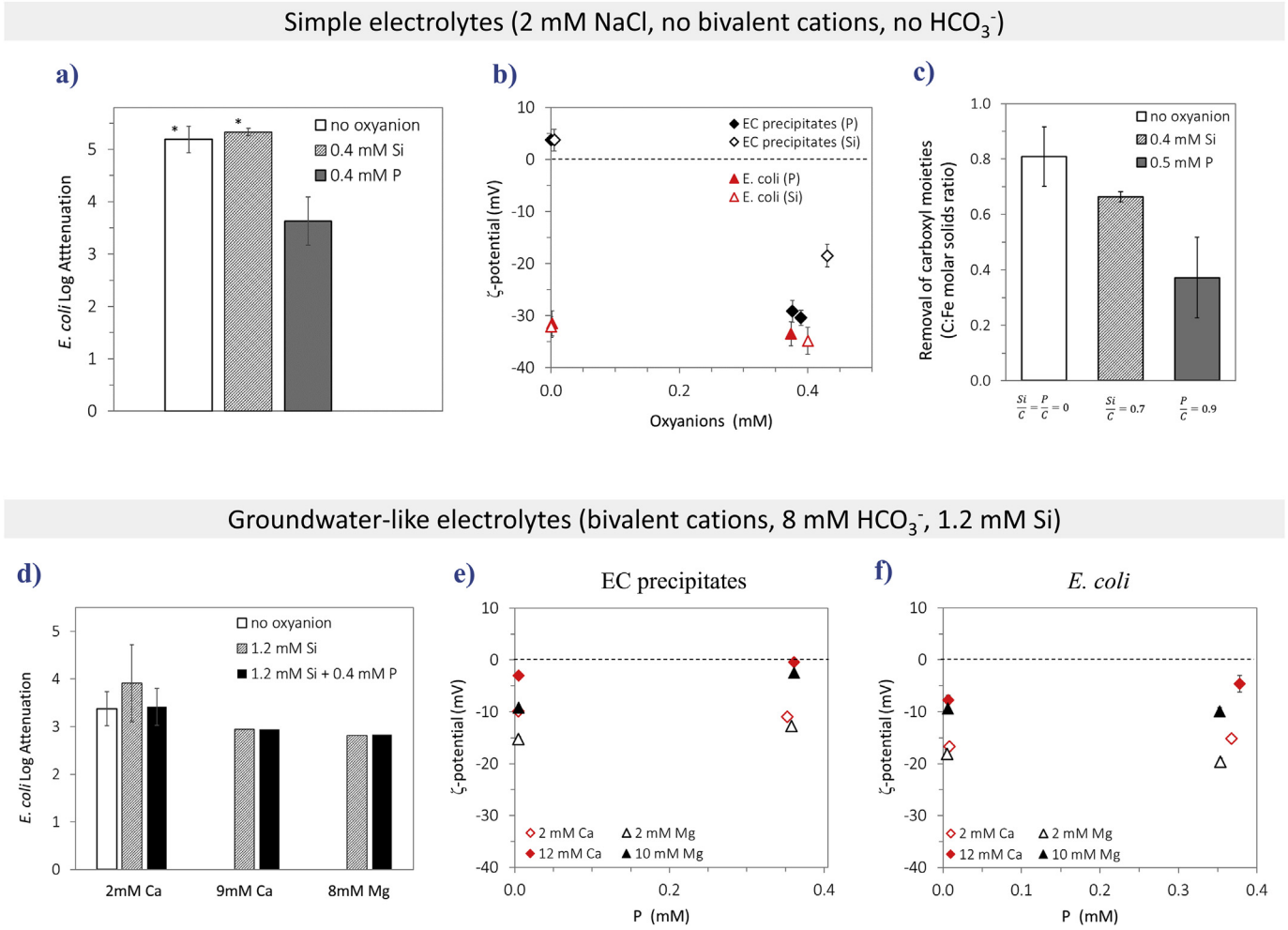

Fig. 3. Effect of P and Si on *E. coli* attenuation by Fe-EC with an Fe dosage of 0.5 mM in single solute electrolytes (0.4 mM P or Si in 2 mM NaCl background for conductivity; panels a, b and c) and groundwater-like electrolytes containing 8 mM HCO_3^-, 1.2 mM Si, and bivalent cations (panels d, e and f). a) Effect of Si and P on *E. coli* attenuation. Asterisks indicate that the detection limit for bacteria attenuation was reached for some of the replicate experiments. b) Effect of Si (open symbols) and P (solid symbols) on the ζ-potential of EC precipitates and *E. coli* cells. c) Effect of P and Si on the removal of citrate (a proxy for carboxyl moieties) by Fe-EC. d) Effect of P on *E. coli* attenuation at different levels of Ca/Mg. e) Effect of P on the ζ-potential of EC precipitates. f) Effect of P on the ζ-potential of *E. coli* cells. All experiments were conducted at pH 7.0.

bacteria removal in the presence of P cannot be explained by the decrease in precipitate surface charge. Rather, the results in Fig. 3a indicate that inorganic aqueous P competes with bacterial functional groups involved in bonding to EC precipitates. By contrast, our results indicate that Si does not strongly compete with these functional groups.

Because aqueous P and bacterial phosphate groups are structurally and chemically similar, they are expected to compete for precipitate surfaces. However, the competition between P and carboxyl groups is less straight-forward. To assess the effect of P on the adsorption of carboxyl moieties, we measured the removal of citrate (a proxy for carboxyl groups) by Fe-EC in the presence and absence of P. As shown in Fig. 3c, P decreased citrate removal by nearly 54% (initial P:C molar ratio of 0.9). In *E. coli* attenuation experiments, the molar ratio of aqueous P to bacterial surface carboxyl groups is ~2500 mol P: mol C (see Supporting Information). Therefore, aqueous P is expected to strongly compete with bacterial carboxyl groups in attenuation experiments.

Fe(III) (oxyhydr)oxides have a much higher affinity for P than for Si (Li et al., 2014; Roberts et al., 2004). Therefore, Si is not expected to effectively compete with bacterial phosphate groups for precipitate surfaces. In contrast, Fig. 3c shows that Si decreased citrate removal in Fe-EC by nearly 20% (initial Si:C molar ratio of 0.7). In *E. coli* attenuation experiments, where the molar ratio of Si to bacterial surface carboxyl groups is orders of magnitude higher (~2500, see Supporting Information), it is thus likely that Si would inhibit bacteria removal if carboxyl groups played an important role in the adhesion of EC precipitates. Because Si had no detectable effect on *E. coli* attenuation (Fig. 3a), we propose that phosphate groups are the primary sites for the adhesion of EC precipitates to cell walls, with negligible contributions from carboxyl groups.

3.4.2. Groundwater-like electrolytes (with bivalent cations, HCO_3^-, and Si)

In Fig. 3d, we show the effect of P (0–0.4 mM) on *E. coli* attenuation in the presence of Ca (2 and 9 mM) or Mg (8 mM) in a groundwater-like electrolyte containing 8 mM HCO_3^- and 1.2 mM Si. In contrast to experiments in electrolytes free of bivalent cations, where P decreased *E. coli* removal by 1.6 log (Fig. 3a), 0.4 mM P had no effect on *E. coli* removal in the presence of Ca/Mg. We note that lower *E. coli* attenuations in Fig. 3d compared to Fig. 3a (~−2 log) are due to the inhibition of inactivation by 8 mM HCO_3^- (shown in Section 3.1) and to the reduction in removal caused by Ca/Mg (shown in Section 3.3).

Fig. 3e and f show ζ-potential measurements of EC precipitates and *E. coli* cells, respectively, as a function of P concentration in the groundwater-like electrolyte containing bivalent cations. Fig. 3f shows that P did not interact significantly with bacterial cells, as expected. In contrast to single oxyanion systems (Fig. 3b), EC precipitates in the groundwater-like electrolyte were negatively charged for all P concentrations (Fig. 3e), due to sorbed Si/P. In addition, the ζ-potential of EC precipitates did not decrease when the P concentration increased from 0 to 0.4 mM, despite substantial P uptake by precipitates (P:Fe molar solids ratios of 0.6–0.8, see Table S4). This result stands in strong contrast with electrolytes containing no Ca/Mg, where high concentrations of P (0.4 mM) and similar P:Fe solids ratios (0.6 mol:mol) significantly decreased EC precipitate surface charge (Fig. 3b). In the groundwater-like electrolytes, ICP-OES measurements indicated that Ca/Mg uptake by EC precipitates increased by 20–200% –depending on the initial Ca/Mg concentration – in the presence of 0.4 mM P (Table S4). This co-sorption of Ca/Mg explains the negligible impact of P sorption on the surface charge of EC precipitates.

Based on the co-sorption of Ca/Mg and P, the behavior of precipitate and bacteria surfaces, and the negligible effect of P on *E. coli* removal observed in our system, we propose that Ca/Mg can act as a bivalent cation bridge between bacterial phosphate groups and P sorbed to EC precipitates. Specifically, we propose that Ca–P–Fe or Mg–P–Fe complexes, which are consistent with Ca–P–Fe configurations previously documented in comparable electrolytes in the absence of bacteria (Senn et al., 2015; van Genuchten et al., 2014a; Voegelin et al., 2010), create additional sites at the precipitate surface that can interact with bacterial cell walls.

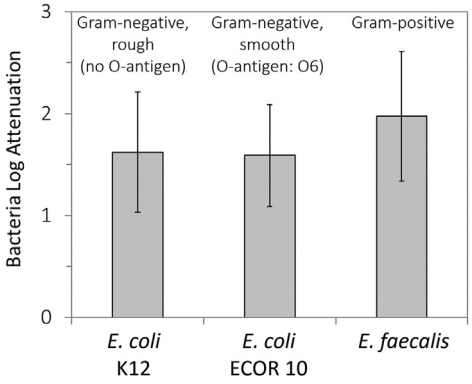

Fig. 4. Log attenuation of three different bacterial strains by Fe-EC, at an Fe dosage of 0.5 mM. All experiments were conducted at pH 7.5 in SBGW (8.2 mM HCO_3^-, 2.7 mM Ca, 2.0 mM Mg, 1.3 mM Si, 0.15 mM P, and 6.3 μM As(III)). The log attenuation of *E. coli* K12 in SBGW shown here has also been reported elsewhere (Delaire et al., 2015).

3.5. Attenuation of different types of bacteria

The attenuation of *E. coli* K12, *E. coli* ECOR 10, and *E. faecalis* in SBGW with an Fe dosage of 0.5 mM is shown in Fig. 4. No significant difference between the log attenuations of the three different bacterial strains was observed, despite their considerably different cell wall structures. For example, the surface of Gram-positive *E. faecalis* is composed of a peptidoglycan layer topped with techoic acids, whereas the surface of Gram-negative *E. coli* is made of phospholipids and lipopolysaccharides (LPS) (Madigan et al., 2000). Furthermore, the two *E. coli* strains differ by the length of their LPS: ECOR 10 is a smooth strain with a full-length LPS (with O-antigen), whereas K12 is a rough strain with a truncated LPS (no O-antigen). Such differences in cell wall composition lead to differences in hydrophobicity, surface charge, surface roughness, and steric hindrance to approach mineral surfaces and nanoparticles (Chen and Walker, 2012; Jacobson et al., 2015; Walker et al., 2004).

Previous studies have found that cell wall composition and LPS length affect the interactions of bacteria with mineral surfaces (sand, iron-oxide coated sand, and gold nanoparticles) in systems governed by non-specific interactions, such as electrostatic, steric, hydrophobic, and van der Waals forces (Chen and Walker, 2012; Jacobson et al., 2015; Mohanty et al., 2013; Truesdail et al., 1998; Walker et al., 2004). In contrast to these studies, similar attenuation of *E. coli* K12, *E. coli* ECOR 10, and *E. faecalis* in our system is likely due to the dominant role of specific interactions in bacteria-precipitate adhesion. The literature shows that all bacterial cell walls are very similar in terms of functional groups (Borrok et al., 2005 and references therein). Specifically, phosphate functional groups, which we found to be the primary binding sites for EC precipitates on *E. coli*, are present in comparable abundance on Gram-negative and Gram-positive bacteria (Borrok et al., 2005) (mainly on phospholipids and on techoic acids, respectively), which is consistent with similar removal of *E. coli* and *E. faecalis*. In

addition, negligible steric hindrance from longer LPS on *E. coli* is likely due to the small size of EC precipitates compared to bacterial cells (Fig. S4).

These results suggest that Fe-EC would be similarly effective for all waterborne pathogenic bacteria, both Gram-negative (e.g. *Vibrio cholera*, *Shigella*, *Salmonella*, pathogenic *E. coli*) and Gram-positive (e.g. *E. faecalis*, *Bacillus cereus*, *Staphylococcus aureus*). Finally, similar attenuation of *E. coli* K12 and *E. coli* ECOR 10 suggests that fecal pathogens, which are typically smooth strains (Felix and Pitt, 1935), would be as effectively removed as our model indicator *E. coli* K12. Overall, these results are promising for the application of Fe-EC to drinking water or wastewater treatment.

4. Conclusions

In this study, we showed that bacteria inactivation, which can be significant in the absence of oxidant scavengers, is largely suppressed by HCO_3^- concentrations characteristic of natural waters. Therefore, we expect physical removal to be the primary process of bacteria attenuation in most water treatment applications.

We have shown that removal is driven by the interactions of EC precipitates with bacterial phosphate groups, which may bind to Fe(III) surfaces directly or via a Ca/Mg bridge to P sorbed on precipitates. These mechanisms are consistent with the minimal impact of ionic strength, which is not expected to affect significantly such specific interactions (Sposito, 2008). In light of these mechanisms, the contrasted effects of P and Si observed in this study can be generalized to other strongly- (e.g., arsenate) and weakly- (e.g., borate, arsenite, nitrate) sorbing oxyanions, respectively. Similarly, the observed impact of Ca/Mg (hardness) can be extrapolated to metallic bivalent cations that may be present in wastewater, such as Cu^{2+}, Cd^{2+}, Pb^{2+}, and Zn^{2+}. Natural organic matter (NOM) has been found to inhibit virus attenuation by Fe-EC (Tanneru and Chellam, 2012). However, because NOM mainly bears carboxyl and hydroxyl moieties (Chen et al., 2002; Driver and Perdue, 2014), which have a lower sorption affinity for Fe(III) (oxyhydr)oxides than bacterial phosphate groups, it is not expected to inhibit bacteria removal by Fe-EC significantly, consistent with our previous finding in synthetic Bengal groundwater (Delaire et al., 2015). Finally, extracellular polymeric substances (EPS), in which environmental bacteria are typically embedded, are not expected to affect the adhesion of EC precipitates significantly, because EPS contain phosphate functional groups that can form bonds with Fe(III) oxides (Omoike et al., 2004), similar to bacterial cell walls.

Consistent with the universal presence of phosphate groups on bacteria surfaces, Fe-EC is equally effective towards Gram-positive and Gram-negative bacteria, rough and smooth alike. Our results strongly suggest that Fe-EC, which is a technology applicable to decentralized arsenic remediation in low-resource settings (Amrose et al., 2014; Holt et al., 2005), can also effectively remove all types of bacterial contamination from a wide range of groundwater sources. Field validation of these promising results as well as an investigation of virus attenuation are needed to confirm the potential of Fe-EC to substitute for existing disinfection methods when applied to groundwater treatment.

Acknowledgements

This work was supported by the Development Impact Lab (USAID Cooperative Agreement AID-OAA-A-13-00002), part of the USAID Higher Education Solutions Network, and the Andrew and Virginia Rudd Family Foundation Chair for Safe Water and Sanitation administered by the Blum Center for Developing Economies. Additionally, C.M.v.G. acknowledges funding support from the Netherlands Organization for Scientific Research (NWO) through a Veni grant (proposal #14400). We wish to express our gratitude to Kara Nelson, who provided useful discussions regarding the complexation of Ca/Mg to bacterial functional groups, and to David Sedlak, Denise Schichnes, John Wertz, and Aidan Cecchetti for their kind assistance along various steps of this work. ζ-potential measurements were conducted at the Molecular Foundry of Lawrence Berkeley National Laboratory and supported by the Office of Science, Office of Basic Energy Sciences, of the U.S. Department of Energy under Contract No. DE-AC02-05CH11231.

Appendix A. Supplementary data

Supplementary data related to this article can be found at http://dx.doi.org/10.1016/j.watres.2016.07.020.

References

Alt, E., Leipold, F., Milatovic, D., Lehmann, G., Heinz, S., Schömig, A., 1999. Hydrogen peroxide for prevention of bacterial growth on polymer biomaterials. Ann. Thorac. Surg. 68, 2123–2128. http://dx.doi.org/10.1016/S0003-4975(99)00832-2.

Amrose, S.E., Bandaru, S.R.S., Delaire, C., van Genuchten, C.M., Dutta, A., DebSarkar, A., Orr, C., Roy, J., Das, A., Gadgil, A.J., 2014. Electro-chemical arsenic remediation: field trials in West Bengal. Sci. Total Environ. 488–489, 539–546. http://dx.doi.org/10.1016/j.scitotenv.2013.11.074.

Appenzeller, B.M.R., Duval, Y.B., Thomas, F., Block, J.-C., 2002. Influence of phosphate on bacterial adhesion onto iron oxyhydroxide in drinking water. Environ. Sci. Technol. 36, 646–652. http://dx.doi.org/10.1021/es010155m.

Arai, Y., Sparks, D.L., 2001. ATR–FTIR spectroscopic investigation on phosphate adsorption mechanisms at the ferrihydrite–water interface. J. Colloid Interface Sci. 241, 317–326. http://dx.doi.org/10.1006/jcis.2001.7773.

Augusto, O., Miyamoto, S., 2011. Oxygen radicals and related species. Ohara Augusto – Academia.edu. In: Pantopoulos, H.M. (Ed.), Principles of Free Radical Biomedicine, vol. 1. Nova Science Publishers, Inc.

Barrera-Díaz, C., Ureña-Nuñez, F., Campos, E., Palomar-Pardavé, M., Romero-Romo, M., 2003. A combined electrochemical-irradiation treatment of highly colored and polluted industrial wastewater. Radiat. Phys. Chem. 67, 657–663. http://dx.doi.org/10.1016/S0969-806X(02)00497-8.

Beveridge, T.J., Koval, S.F., 1981. Binding of metals to cell envelopes of Escherichia coli K-12. Appl. Environ. Microbiol. 42, 325–335.

Borrok, D., Turner, B.F., Fein, J.B., 2005. A universal surface complexation framework for modeling proton binding onto bacterial surfaces in geologic settings. Am. J. Sci. 305, 826–853. http://dx.doi.org/10.2475/ajs.305.6-8.826.

Chan, C.S., Fakra, S.C., Edwards, D.C., Emerson, D., Banfield, J.F., 2009. Iron oxyhydroxide mineralization on microbial extracellular polysaccharides. Geochim. Cosmochim. Acta 73, 3807–3818.

Chassé, A.W., Ohno, T., Higgins, S.R., Amirbahman, A., Yildirim, N., Parr, T.B., 2015. Chemical force spectroscopy evidence supporting the layer-by-layer model of organic matter binding to iron (oxy)Hydroxide mineral surfaces. Environ. Sci. Technol. 49, 9733–9741. http://dx.doi.org/10.1021/acs.est.5b01877.

Chen, G., Walker, S.L., 2012. Fecal indicator bacteria transport and deposition in saturated and unsaturated porous media. Environ. Sci. Technol. 46, 8782–8790. http://dx.doi.org/10.1021/es301378q.

Chen, J., Gu, B., Leboeuf, E.J., Pan, H., Dai, S., 2002. Spectroscopic characterization of the structural and functional properties of natural organic matter fractions. Chemosphere 48, 59–68.

Delaire, C., van Genuchten, C.M., Nelson, K.L., Amrose, S.E., Gadgil, A.J., 2015. Escherichia coli attenuation by Fe electrocoagulation in synthetic Bengal groundwater: effect of pH and natural organic matter. Environ. Sci. Technol. 49, 9945–9953. http://dx.doi.org/10.1021/acs.est.5b01696.

Driver, S.J., Perdue, E.M., 2014. Advances in the Physicochemical Characterization of Dissolved Organic Matter: Impact on Natural and Engineered Systems, ACS Symposium Series. American Chemical Society, Washington, DC. http://dx.doi.org/10.1021/bk-2014-1160.

Elzinga, E.J., Huang, J.-H., Chorover, J., Kretzschmar, R., 2012. ATR-FTIR spectroscopy study of the influence of pH and contact time on the adhesion of Shewanella putrefaciens bacterial cells to the surface of hematite. Environ. Sci. Technol. 46, 12848–12855. http://dx.doi.org/10.1021/es303318y.

Felix, A., Pitt, R.M., 1935. Virulence and immunogenic activities of *B. Typhosus* in relation to its antigenic constituents. J. Hyg. (Lond) 35, 428–436.

Filius, J.D., Lumsdon, D.G., Meeussen, J.C.L., Hiemstra, T., Van Riemsdijk, W.H., 2000. Adsorption of fulvic acid on goethite. Geochim. Cosmochim. Acta 64, 51–60. http://dx.doi.org/10.1016/S0016-7037(99)00176-3.

Ghernaout, D., Badis, A., Kellil, A., Ghernaout, B., 2008. Application of electrocoagulation in Escherichia coli culture and two surface waters. Desalination 219, 118–125. http://dx.doi.org/10.1016/j.desal.2007.05.010.

Hamid, R.D., Swedlund, P.J., Song, Y., Miskelly, G.M., 2011. Ionic strength effects on silicic acid (H_4SiO_4) sorption and oligomerization on an iron oxide surface: an

interesting interplay between electrostatic and chemical forces. Langmuir 27, 12930–12937. http://dx.doi.org/10.1021/la201775c.
Holt, P.K., Barton, G.W., Mitchell, C.A., 2005. The future for electrocoagulation as a localised water treatment technology. Chemosphere 59, 355–367. http://dx.doi.org/10.1016/j.chemosphere.2004.10.023.
Hug, S.J., Leupin, O., 2003. Iron-catalyzed oxidation of arsenic(III) by oxygen and by hydrogen peroxide: pH-dependent formation of oxidants in the Fenton reaction. Environ. Sci. Technol. 37, 2734–2742.
Ikawa, S., Kitano, K., Hamaguchi, S., 2010. Effects of pH on bacterial inactivation in aqueous solutions due to low-temperature atmospheric pressure plasma application. Plasma Process. Polym. 7, 33–42. http://dx.doi.org/10.1002/ppap.200900090.
Jacobsen, F., Holcman, J., Sehested, K., 1998. Reactions of the ferryl ion with some compounds found in cloud water. Int. J. Chem. Kinet. 30, 215–221. http://dx.doi.org/10.1002/(SICI)1097-4601(1998)30:3<215::AID-KIN7>3.0.CO;2-V.
Jacobson, K.H., Gunsolus, I.L., Kuech, T.R., Troiano, J.M., Melby, E.S., Lohse, S.E., Hu, D., Chrisler, W.B., Murphy, C.J., Orr, G., Geiger, F.M., Haynes, C.L., Pedersen, J.A., 2015. Lipopolysaccharide density and structure govern the extent and distance of nanoparticle interaction with actual and model bacterial outer membranes. Environ. Sci. Technol. 49, 10642–10650. http://dx.doi.org/10.1021/acs.est.5b01841.
Johnson, K.J., Szymanowski, J.E.S., Borrok, D., Huynh, T.Q., Fein, J.B., 2007. Proton and metal adsorption onto bacterial consortia: stability constants for metal–bacterial surface complexes. Chem. Geol. 239, 13–26.
Kanematsu, M., Young, T.M., Fukushi, K., Green, P.G., Darby, J.L., 2013. Arsenic(III, V) adsorption on a goethite-based adsorbent in the presence of major co-existing ions: modeling competitive adsorption consistent with spectroscopic and molecular evidence. Geochim. Cosmochim. Acta 106, 404–428. http://dx.doi.org/10.1016/j.gca.2012.09.055.
Keenan, C.R., Sedlak, D.L., 2008. Factors affecting the yield of oxidants from the reaction of nanoparticulate zero-valent iron and oxygen. Environ. Sci. Technol. 42, 1262–1267. http://dx.doi.org/10.1021/es7025664.
Kelly, S.D., Hesterberg, D., Ravel, B., 2008. Analysis of soils and minerals using X-ray absorption spectroscopy. In: Methods of Soil Analysis. Part 5. Mineralogical Methods.
Kim, J.Y., Park, H.-J., Lee, C., Nelson, K.L., Sedlak, D.L., Yoon, J., 2010. Inactivation of Escherichia coli by nanoparticulate zerovalent iron and ferrous ion. Appl. Environ. Microbiol. 76, 7668–7670. http://dx.doi.org/10.1128/AEM.01009-10.
Li, L., Li, J., Shao, C., Zhang, K., Yu, S., Gao, N., Deng, Y., Yin, D., 2014. Arsenic removal in synthetic ground water using iron electrolysis. Sep. Purif. Technol. 122, 225–230. http://dx.doi.org/10.1016/j.seppur.2013.11.012.
Li, L., van Genuchten, C.M., Addy, S.E.A., Yao, J., Gao, N., Gadgil, A.J., 2012. Modeling As(III) oxidation and removal with iron electrocoagulation in groundwater. Environ. Sci. Technol. 46, 12038–12045. http://dx.doi.org/10.1021/es302456b.
Madigan, M.T., Martinko, J.M., Parker, J., 2000. Brock Biology of Microorganisms. Prentice Hall, Upper Saddle River NJ.
Mazel, D., Dychinco, B., Webb, V.A., Davies, J., 2000. Antibiotic resistance in the ECOR collection: integrons and identification of a novel aad gene. Antimicrob. Agents Chemother. 44, 1568–1574.
McBride, M.B., Kung, K.-H., 1991. Adsorption of phenol and substituted phenols by iron oxides. Environ. Toxicol. Chem. 10, 441–448. http://dx.doi.org/10.1002/etc.5620100403.
Medinas, D.B., Cerchiaro, G., Trindade, D.F., Augusto, O., 2007. The carbonate radical and related oxidants derived from bicarbonate buffer. IUBMB Life 59, 255–262. http://dx.doi.org/10.1080/15216540701230511.
Miot, J., Benzerara, K., Obst, M., Kappler, A., Hegler, F., Schädler, S., Bouchez, C., Guyot, F., Morin, G., 2009. Extracellular iron biomineralization by photoautotrophic iron-oxidizing bacteria. Appl. Environ. Microbiol. 75, 5586–5591. http://dx.doi.org/10.1128/AEM.00490-09.
Mohanty, S.K., Torkelson, A.A., Dodd, H., Nelson, K.L., Boehm, A.B., 2013. Engineering solutions to improve the removal of fecal indicator bacteria by bioinfiltration systems during intermittent flow of stormwater. Environ. Sci. Technol. 47, 10791–10798. http://dx.doi.org/10.1021/es305136b.
Neta, P., Huie, R.E., Ross, A.B., 1988. Rate constants for reactions of inorganic radicals in aqueous solution. J. Phys. Chem. Ref. Data 17, 1027. http://dx.doi.org/10.1063/1.555808.
Ngwenya, B.T., Sutherland, I.W., Kennedy, L., 2003. Comparison of the acid-base behaviour and metal adsorption characteristics of a gram-negative bacterium with other strains. Appl. Geochem. 18, 527–538.
Norén, K., Loring, J.S., Persson, P., 2008. Adsorption of alpha amino acids at the water/goethite interface. J. Colloid Interface Sci. 319, 416–428. http://dx.doi.org/10.1016/j.jcis.2007.11.046.
Omoike, A., Chorover, J., Kwon, K.D., Kubicki, J.D., 2004. Adhesion of bacterial exopolymers to alpha-FeOOH: inner-sphere complexation of phosphodiester groups. Langmuir 20, 11108–11114. http://dx.doi.org/10.1021/la048597+.
Parikh, S.J., Chorover, J., 2006. ATR-FTIR spectroscopy reveals bond formation during bacterial adhesion to iron oxide. Langmuir 22, 8492–8500. http://dx.doi.org/10.1021/la061359p.
Parikh, S.J., Mukome, F.N.D., Zhang, X., 2014. ATR-FTIR spectroscopic evidence for biomolecular phosphorus and carboxyl groups facilitating bacterial adhesion to iron oxides. Colloids Surf. B. Biointerfaces 119, 38–46. http://dx.doi.org/10.1016/j.colsurfb.2014.04.022.
Roberts, L.C., Hug, S.J., Ruettimann, T., Billah, M.M., Khan, A.W., Rahman, M.T., 2004. Arsenic removal with Iron(II) and Iron(III) in waters with high silicate and phosphate concentrations. Environ. Sci. Technol. 38, 307–315. http://dx.doi.org/10.1021/es0343205.
Senn, A.-C., Kaegi, R., Hug, S.J., Hering, J.G., Mangold, S., Voegelin, A., 2015. Composition and structure of Fe(III)-precipitates formed by Fe(II) oxidation in water at near-neutral pH: interdependent effects of phosphate, silicate and Ca. Geochim. Cosmochim. Acta 162, 220–246. http://dx.doi.org/10.1016/j.gca.2015.04.032.
Sposito, G., 2008. The Chemistry of Soils. Oxford University Press.
Stachowicz, M., Hiemstra, T., van Riemsdijk, W.H., 2008. Multi-competitive interaction of As(III) and As(V) oxyanions with Ca(2+), Mg(2+), PO(3-)(4), and CO(2-)(3) ions on goethite. J. Colloid Interface Sci. 320, 400–414. http://dx.doi.org/10.1016/j.jcis.2008.01.007.
STEC center, 2016. STEC Center Website [WWW Document]. URL. http://shigatox.net/new/reference-strains/ecor.html (accessed 01.01.16.).
Stevenson, G., Neal, B., Liu, D., Hobbs, M., Packer, N.H., Batley, M., Redmond, J.W., Lindquist, L., Reeves, P., 1994. Structure of the O antigen of Escherichia coli K-12 and the sequence of its rfb gene cluster. J. Bacteriol. 176, 4144–4156.
Tanneru, C.T., Chellam, S., 2012. Mechanisms of virus control during iron electrocoagulation–microfiltration of surface water. Water Res. 46, 2111–2120. http://dx.doi.org/10.1016/j.watres.2012.01.032.
Truesdail, S., Lukasik, J., Farrah, S., Shah, D., Dickinson, R., 1998. Analysis of bacterial deposition on metal (Hydr)oxide-Coated sand filter media. J. Colloid Interface Sci. 203, 369–378. http://dx.doi.org/10.1006/jcis.1998.5541.
van Genuchten, C.M., Addy, S.E.A., Peña, J., Gadgil, A.J., 2012. Removing arsenic from synthetic groundwater with iron electrocoagulation: an Fe and As K-edge EXAFS study. Environ. Sci. Technol. 46, 986–994. http://dx.doi.org/10.1021/es201913a.
van Genuchten, C.M., Gadgil, A.J., Peña, J., 2014a. Fe(III) nucleation in the presence of bivalent cations and oxyanions leads to subnanoscale 7 Å polymers. Environ. Sci. Technol. 48, 11828–11836. http://dx.doi.org/10.1021/es503281a.
van Genuchten, C.M., Peña, J., Amrose, S.E., Gadgil, A.J., 2014b. Structure of Fe(III) precipitates generated by the electrolytic dissolution of Fe(0) in the presence of groundwater ions. Geochim. Cosmochim. Acta 127, 285–304. http://dx.doi.org/10.1016/j.gca.2013.11.044.
Voegelin, A., Kaegi, R., Frommer, J., Vantelon, D., Hug, S.J., 2010. Effect of phosphate, silicate, and Ca on Fe(III)-precipitates formed in aerated Fe(II)- and As(III)-containing water studied by X-ray absorption spectroscopy. Geochim. Cosmochim. Acta 74, 164–186. http://dx.doi.org/10.1016/j.gca.2009.09.020.
Walker, S.L., Redman, J.A., Elimelech, M., 2004. Role of cell surface lipopolysaccharides in Escherichia coli K12 adhesion and transport. Langmuir 20, 7736–7746. http://dx.doi.org/10.1021/la049511f.
WHO, 2011. WHO | Guidelines for Drinking-water Quality, fourth ed. World Health Organization.
Yan, W., Wang, H., Jing, C., 2016. Adhesion of *Shewanella oneidensis* MR-1 to goethite: a two-dimensional correlation spectroscopic study. Environ. Sci. Technol. 50, 4343–4349. http://dx.doi.org/10.1021/acs.est.6b00066.